AGU PUBLICATIONS

JGR

Journal of Geophysical Research: Earth Surface

RESEARCH ARTICLE
10.1002/2014JF003330

Key Points:
- A discrete element model reproduces rock fragmentation during a rockslide
- The runout of the collapse decreases as the material strength increases
- The runout of a rockslide increases as the fragmentation degree in the deposit increases

Correspondence to:
V. J. Langlois,
vincent.langlois@univ-lyon1.fr

Citation:
Langlois, V. J., A. Quiquerez, and P. Allemand (2015), Collapse of a two-dimensional brittle granular column: Implications for understanding dynamic rock fragmentation in a landslide, *J. Geophys. Res. Earth Surf.*, *120*, 1866–1880, doi:10.1002/2014JF003330.

Received 3 SEP 2014
Accepted 19 AUG 2015
Accepted article online 24 AUG 2015
Published online 22 SEP 2015

Collapse of a two-dimensional brittle granular column: Implications for understanding dynamic rock fragmentation in a landslide

Vincent J. Langlois[1], Amélie Quiquerez[2], and Pascal Allemand[1]

[1]Laboratoire de Géologie de Lyon, Université Claude Bernard Lyon 1/ENS de Lyon/CNRS UMR 5276, Villeurbanne, France, [2]ARTeHIS, Université de Bourgogne/CNRS UMR 6298, Dijon, France

Abstract We investigate numerically the failure, collapse, and flow of a two-dimensional brittle granular column over a horizontal surface. In our discrete element simulations, we consider a vertical monolayer of spherical particles that are initially held together by tensile bonds, which can be irreversibly broken during the collapse. This leads to dynamic fragmentation within the material during the flow. Compared to what happens in the case of a noncohesive granular column, the deposit is much rougher, and the internal stratigraphic structure of the column is not preserved during the collapse. As has been observed in natural rockslides, we find that the deposit consists of large blocks laying on a lower layer of fine fragments. The influence of the aspect ratio of the column on the runout distance is the same as in the noncohesive case. Finally, we show that for a given aspect ratio of the column, the runout distance is higher when the deposit is highly fragmented, which confirms previous hypotheses proposed by Davies et al. (1999).

1. Introduction

1.1. Natural Events and Runout Distance

Gravitational flows are very common events at the surface of the Earth. On land, they constitute the primary processes that supply sediment to river networks [*Lin et al.*, 2008; *Allemand et al.*, 2014]. Rock avalanches, landslides (either subaerial or subaqueous), and debris flows can mobilize solid volumes up to 10^{11} m^3 on Earth and 10^{13} m^3 on Mars or under water [*Legros*, 2002; *Hewitt et al.*, 2008]. On Earth, such flows can travel over several tens of kilometers on land [*Robinson et al.*, 2014] and up to a hundred kilometers under water and are able to transport very large blocks of rock (more than 10 m). Therefore, they constitute a significant natural hazard and may cause major environmental, economic, and social damages. Hence, accurately predicting their behavior is an important issue. However, because they involve the combined motion of a very large number of solid particles and (in most cases) of an interstitial fluid (either air or water), understanding and modeling such events still represent an important challenge for geophysicists.

Among these different types of events, rockslides or rock avalanches may appear simpler since they do not involve a significant amount of water. However, a simple description of energy dissipation by basal solid friction fails to explain the very long runout distances often observed for events of large volume [*Lajeunesse et al.*, 2004]. To go beyond this simplistic approach, the spreading of a granular mass over a given topography has also been modeled by hydrodynamic simulations based on the "shallow-water" assumption. Yet using the classical Savage-Hutter formulation [*Savage and Hutter*, 1991] for the basal shear stress does not lead to an accurate prediction of the shape and volume of the deposit of an avalanche, unless an unrealistic value of the friction angle is chosen or a constant basal shear stress is used [*Mangeney-Castelnau et al.*, 2003; *Kelfoun and Druitt*, 2005; *Kelfoun et al.*, 2009]. In order to account for this, several mechanisms of effective lubrication have therefore been invoked, such as basal melting [*De Blasio and Elverhøi*, 2008], mechanical or acoustic fluidization [*Davies*, 1982; *Collins and Melosh*, 2003], size segregation [*Roche et al.*, 2005], progressive entrainment of material during the flow [*Mangeney et al.*, 2007], and dynamic rock fragmentation [*Davies et al.*, 1999; *Davies and McSaveney*, 2009; *Davies et al.*, 2010].

1.2. Collapse of a Granular Column

In the last decade, several experimental investigations have been performed on a simplified analogue model of a landslide: the collapse of a granular column on a horizontal surface. These experiments offer a simple and

straightforward way to assess the runout distance of a flowing granular mass as a function of a small number of control parameters. Similar experiments have been performed either in air [*Lube et al.*, 2004; *Balmforth and Kerswell*, 2005; *Lajeunesse et al.*, 2004, 2005], under water [*Thompson and Huppert*, 2007], or with air-fluidized grains [*Roche et al.*, 2011], and both in axisymmetric and quasi-2-D configurations. On the same problem, numerical simulations have been developed [*Staron and Hinch*, 2005; *Zenit*, 2005; *Staron*, 2008; *Crosta et al.*, 2009], using mostly the contact dynamics method [*Moreau*, 1994], in order to explore the parameter space and to help in developing analytical models [*Larrieu et al.*, 2006; *Doyle et al.*, 2007]. Recently, *Lagrée et al.* [2011] applied a continuum approach to the modeling of the collapse of a column, using the granular rheology introduced by *Jop et al.* [2006].

These studies showed that the runout distance normalized by the initial width of the column can be simply expressed as a power law function of the initial aspect ratio of the column. The prefactor of this power law (but not its exponent) depends on the nature of the granular material (surface roughness, angle of repose...) [*Balmforth and Kerswell*, 2005]. Large events such as Martian landslides appear to follow the same power laws but with a higher prefactor than in experiments and simulations: their runout distances can therefore be twice longer than predicted values [*Lajeunesse et al.*, 2006; *Roche et al.*, 2011].

1.3. Fragmentation in Rockslides

Aside from its simplified geometry, the main limitation of the granular column experiment is that the flowing material is already fragmented before the collapse. By contrast, in natural conditions the volume of rock is initially roughly cohesive before failing: it is only during the flow that rocks experience multiple fragmentations. As a consequence, the deposit of a rockslide usually consists of a very wide range of fragment sizes (from nanometers to meters): the subsurface material in long runout rock avalanches has been observed in diverse geological conditions to be composed of highly fragmented parent material [*Cruden and Hungr*, 1986; *Ui et al.*, 1986; *Fauque and Strecker*, 1988; *Glicken*, 1998; *Schneider and Fisher*, 1998]. This wide size distribution results in particle segregation by size: the largest particles usually accumulate at the front and at the surface of the deposit, laying on top of a basal layer of finer particles [*Cruden and Hungr*, 1986; *Hewitt*, 1988; *Yarnold*, 1993; *Davies et al.*, 1999; *Bernard et al.*, 2009]. Dynamic rock fragmentation within the flow has been invoked as a possible mechanism for effective lubrication in debris avalanches of large volume [*Davies et al.*, 1999, 2006; *Davies and McSaveney*, 2009; *McSaveney and Davies*, 2009; *Davies et al.*, 2010]. On the other hand, *Locat et al.* [2006] and *Crosta et al.* [2007] estimate that the energy consumed by fragmentation processes represents a significant fraction of the available potential energy (up to 20 or 30%), which would imply that fragmentation reduces the runout of a rockslide. These contradictory results suggest that it would be worth investigating directly the effect of fragmentation in the simple gravitational collapse of a column. Instead of using an initially granular material (as sand), the material should be initially solid and disintegrate into fragments during the collapse. This can be achieved if grains are initially held together by cohesive bonds, which can be broken during the collapse.

1.4. Collapse of a Brittle Column

The role of cohesive forces in granular packings and flows has already been investigated numerically [*Taylor et al.*, 2008], experimentally [*Mason et al.*, 1999; *Mériaux and Triantafillou*, 2008; *Métayer et al.*, 2010; *Lumay and Vandewalle*, 2010; *Artoni et al.*, 2013], and theoretically [*Restagno et al.*, 2004]. However, in these studies the cohesive force is restored each time two particles come again in contact. This is not the case in a rockslide: when a rock is crushed into several pieces, broken bonds are not restored. Such an irreversible fragmentation of rocks is difficult to achieve in experiments. By using a geotechnical centrifuge, *Bowman et al.* [2012] studied the fragmentation of avalanching coal blocks under high effective gravity (up to 50g) and managed to measure the final degree of breakage in the material. If normalized by the cubic root of the mobilized volume, the runout length appears to increase linearly with the relative breakage of material in the final deposit. The authors successfully compare this result with a few observations available in natural events. However, a complete parametric study is difficult to achieve in this type of experiment, and the final degree of fragmentation remains quite low compared to natural examples.

In order to complement this experimental investigation, and to go beyond the model of the granular column, we developed a numerical simulation for the collapse of a brittle column. Our model relies upon a discrete element method which has already been proved to reproduce correctly dry granular flows (with no fragmentation) in various geometries [*Silbert et al.*, 2001; *Bi et al.*, 2005; *Taberlet et al.*, 2008; *Morgan and McGovern*, 2005a, 2005b]. In addition to classical granular interactions (friction and repulsion), we add tensile bonds

Table 1. List of the Physical Parameters Used in the Simulations

Variable	Meaning
H_0	initial height of the column
L_0	initial length of the column
L_∞	final length of the deposit
$a = H_0/L_0$	aspect ratio of the brittle column
$\eta = (L_\infty - L_0)/L_0$	normalized runout distance
η_0	normalized runout distance in the granular case
g	gravity
R_0	average radius of the spherical particles
δ	polydispersity of particle sizes
m_0	mass of a particle of radius R_0
k_n	elastic constant of a particle
γ	effective viscosity of a particle
μ	friction coefficient
C	attractive force exerted by tensile bonds
$R_c = 0.25R_0$	threshold of bond rupture
$\mathrm{Bo} = C/(m_0 g)$	granular Bond number
ϵ	volumetric fraction of fine fragments
Φ	degree of fragmentation
τ_{ff}	free-fall timescale

between grains that can be irreversibly broken if grains are spread apart. Compared to a continuum model, which can compute an effective rheology for a divided material, this discrete approach permits an explicit representation of fragmentation, since each fragment is modeled by a distinct element. Contrary to a classical granular model, it also allows to model the initial column or large fragments as having a given tensile strength.

The present article is organized as follows: the next section presents the numerical method used in our simulations; section 3 discusses the runout distance and the dynamics of fragmentation during the collapse; and in section 4 we describe the characteristics of the deposit.

2. Numerical Model

We developed a new numerical code that simulates the two-dimensional motion of 10,000 spherical unit particles confined in a 2-D plane, using the classical numerical methods of molecular dynamics [*Cundall and Strack*, 1979; *Silbert et al.*, 2001; *Pöschel and Schwager*, 2005]. The translational motion of these spheres is restricted to the $(x; z)$ plane while they can only rotate around the y axis, which makes their dynamics similar to those of disks or rods. We do not account for the influence of the interstitial fluid, which means that the simulations are comparable to a purely dry rock avalanche where the role of air would be neglected. Let us note that the motion of particles is purely two dimensional and that there is no frictional effect exerted by any confining plates, contrary to what happens in quasi-2-D experiments or some 3-D simulations [*Lacaze et al.*, 2008]. Particles experience their own weight and contact forces with one another. At each time step, all forces acting on each particle are computed, and Newton's equations of motion (both rotational and translational) are integrated for all particles simultaneously by the Verlet method. The iterative time step is $\Delta t = \tau_c/100$, with τ_c the typical duration of a collision between particles, which allows the dynamics of each collision to be accurately computed (see numerical details in Appendix 1). In the following we first present the geometry of the numerical setup; then we detail all forces that act on particles; finally, we analyze the properties of the material represented by this model. The list of all parameters used in the model is presented in Table 1.

2.1. Numerical Setup

The column is built in three steps:

1. All particles are placed on a rectangular grid. The radius R_i of each particle is chosen randomly within a narrow uniform distribution between $R_0(1-\delta)$ and $R_0(1+\delta)$, with $\delta = 15\%$. This limited dispersion prevents any ordered distribution of the particles ("crystallization") during the settling phase.

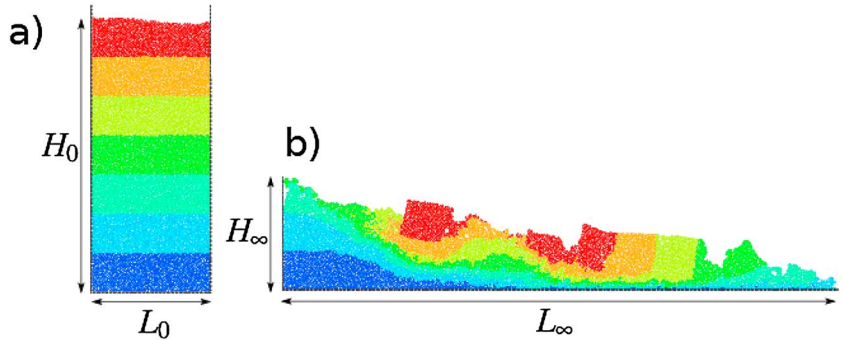

Figure 1. Example of a column (a) before and (b) after its collapse, for Bo = 20. The color indicates the vertical origin of each unit particle.

2. Gravity is switched on, which makes particles settle down between two vertical walls. These walls as well as the horizontal plane are made of immobile particles of radius R_0 (with the same mechanical properties as the mobile particles) and therefore possess a moderate natural roughness. During this settling phase, particles only experience friction and repulsive forces.
3. Once the particles are at rest, a tensile bond is defined between particles that are in contact or nearly in contact (see section 2.2.3). Bonded particles continue to experience an attractive force until they are spread apart by more than $R_c = R_{0/4}$ (see equation (5)). This procedure produces a rectangular column of width L_0 and height H_0 (see Figure 1a). We define the initial aspect ratio as $a = H_0/L_0$.

Once the cohesive column is at rest, the right-side wall is instantaneously removed: the column fails, collapses, and flows rightward. Once the flow has stopped, we characterize the final deposit by its horizontal extent L_∞ and its maximal height H_∞ (see Figure 1b).

2.2. Interactions Between Particles

2.2.1. Repulsive Force

Two particles i and j are in contact when the distance between their centers $|\mathbf{r}_j - \mathbf{r}_i|$ is smaller than the sum of their radii $R_i + R_j$, i.e., $\delta_{ij} = (R_i + R_j) - |\mathbf{r}_j - \mathbf{r}_i| \geq 0$ (see Figure 2). In this case, they interact via a simple spring-dashpot force model: the force exerted by particle j on particle i reads

$$\mathbf{F}_{ij}^{r} = \left[k_n \, \delta_{ij} - \gamma \, \frac{\mathrm{d}\delta_{ij}}{\mathrm{d}t} \right] \mathbf{n}_{ij}. \tag{1}$$

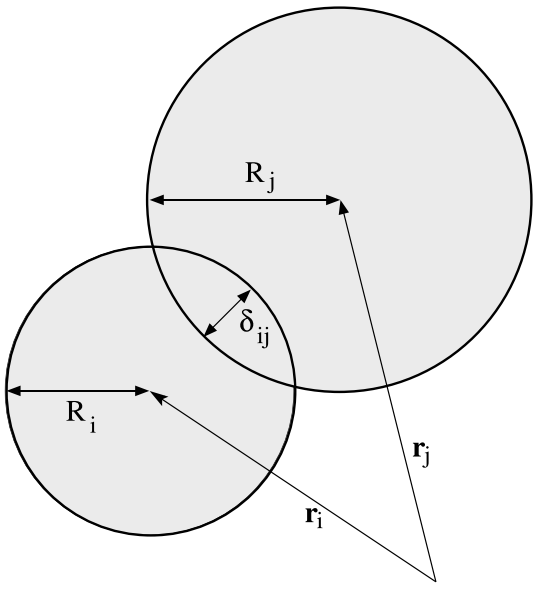

Figure 2. Overlap δ_{ij} between two particles of radii R_i and R_j, located at $\mathbf{r_i}$ and $\mathbf{r_j}$, respectively.

Here k_n is the coefficient of normal elasticity, γ is an effective viscosity that induces energy dissipation during the collision, and $\mathbf{n}_{ij}$ is the normal vector between particle centers: $\mathbf{n}_{ij} = (\mathbf{r}_j - \mathbf{r}_i)/|\mathbf{r}_j - \mathbf{r}_i|$. The values of k_n and γ determine the Young's modulus of the material and the coefficient of restitution in a collision between two particles (see section 2.3). Though the repulsive force between two spheres is supposed to be Hertzian (that is, to scale as $\delta^{3/2}$), it is numerically easier to adopt such a linear repulsive force, since the duration of a collision becomes independent of the relative velocity of particles. It has been shown that this approximation has very little influence on the dynamics of a granular flow [see, for instance, *Schäfer et al.*, 1996; *Silbert et al.*, 2001; *Bi et al.*, 2005] for a given coefficient of restitution.

2.2.2. Solid Friction

Two colliding particles also experience a frictional force, which opposes their relative tangential motion. It is expressed as [*Cundall and Strack*, 1979; *Pöschel and Schwager*, 2005]

$$\mathbf{F}_{ij}^{\ t} = -\min(k_t u_t; \mu\,|\mathbf{F}_{ij}^{\ n}|)\,|\mathbf{v}_{\mathbf{ij}}^{s}| \tag{2}$$

where $\mathbf{v}_{ij}^{\ s}$ is the sliding velocity at the contact, which is a function of the two particles' translational and angular velocities (see equation (A5)). The local friction coefficient is $\mu = 0.6$, and $\mathbf{F}_{ij}^{\ n}$ is the normal force experienced by the two particles. The tangential elastic constant is k_t, and the tangential displacement is u_t, which depends on the history of the contact:

$$u_t = \int_{\text{collision}} |\mathbf{v}_{\mathbf{ij}}^{s}|\mathrm{d}t \tag{3}$$

The ratio k_t/k_n is related to the Poisson ratio of the material. It has been shown that the granular dynamics are not very sensitive to its value and we choose $k_t/k_n = 2/7$ to equal normal and tangential periods of oscillation [*Schäfer et al.*, 1996; *Silbert et al.*, 2001].

2.2.3. Tensile Bonds

In addition to the tangential and repulsive forces, particles that have remained nearly in contact since the beginning of the collapse are linked by a tensile bond and experience attractive forces. Several models of cohesive materials based on discrete elements have already been proposed [*Abe and Mair*, 2005; *Carmona et al.*, 2008]: bonded particles are usually connected via beam-truss elements that can deform in elongation, shear, bending, and torsion. In order to keep our simulations simple and to restrict our study to a single control parameter for the material's strength, we simplify this model and adopt a simplistic expression for the force acting between two bonded particles *i* and *j*:

$$\mathbf{F}_{ij}^{\ c} = -C\mathbf{n}_{ij} \tag{4}$$

where C is the strength of the tensile bond. This approach can be seen as similar to the model for cohesive granular material proposed by *Rognon et al.* [2008], with the difference that in our case no new bonds can be formed during the flow. Two particles are considered to be bonded at a time t if they have remained nearly in contact since the beginning of the simulation, that is, if

$$\forall\, t' \le t\,,\ |\mathbf{r}_j(t') - \mathbf{r}_i(t')| - (R_i + R_j) < R_c = 0.25\,R_0 \tag{5}$$

The threshold $R_c > 0$ ensures that each particle is potentially glued to up to six neighbors, whereas a cohesion strictly by contact would connect a smaller number of particles. If the gap between two bonded particles becomes larger than R_c, the bond is destroyed. For a two-particle fragment and with the chosen value of R_c, this corresponds to a yield strain of 0.06. Let us insist on the fact that the breakage of a bond is irreversible: no new cohesive contacts are formed during the collapse. The instantaneous breakage of a bond implies that its energy is released instantaneously as heat, which is consistent with experimental measurement on the propagation of fractures by *Gross et al.* [1993] or *Sharon et al.* [1996]. Let us note, however, that the tensile strength of our material remains very small compared to its elastic modulus (see section 2.3). Since it has been shown by *Reznichenko et al.* [2012] that submicron particles can agglomerate within a rock avalanche, this assumption remains reasonable only if we model particles of relatively large size (see section 2.3). In the collapse of a column, the only external energy provided to the system, which contributes to the breakage of bonds, is the gravitational energy. Therefore, the relevant nondimensional parameter that characterizes cohesion is the granular Bond number

$$\mathrm{Bo} = \frac{C}{m_0 g} \tag{6}$$

where $m_0 g$ is the weight of a grain of mean radius R_0. This parameter is classically used in the context of cohesive granular materials or powders: the magnitude of the cohesive force is compared either to gravity [*McCarthy et al.*, 2000; *Nase et al.*, 2001] or to the average normal force if gravity does not drive the system [*Rognon et al.*, 2008]. In this study Bo varies from 0 (granular material) to 100 (strong material). In the next section, we compute the corresponding mechanical properties of the material.

Table 2. Height, Width, and Basal Pressure of the Brittle Column as a Function of the Aspect Ratio, for Particles of Mean Size $R_0 = 0.5$ m

a	H_0	L_0	σ_{max}
0.43	65 m	150 m	1.3 MPa
0.96	96 m	100 m	1.9 MPa
3.18	175 m	55 m	3.4 MPa
16.1	403 m	25 m	7.9 MPa

2.3. Mechanical Properties of the Material

Let us now relate the forces acting at the scale of particles to the macroscopic mechanical properties of the material. In order to model a column of realistic height, we need to choose a rather large size for the unit particles. If we choose a mean radius $R_0 = 0.5$ m and a solid density $\rho_s = 2500$ kg m^{-3}, Table 2 gives the height and width of the column for a few values of the aspect ratio, as well as the resulting pressure at the bottom of the column $\sigma_{max} = \rho g H_0$, with $\rho = 0.8\rho_s$ the average bulk density (the average porosity being 20%).

Table 3 summarizes the mechanical properties of individual particles. We adopt an elastic constant $k_n = 10^{10}$ N m^{-1}. Assuming that the Poisson's ratio verifies $\nu^2 \ll 1$ [*Gercek*, 2007], this corresponds to an elastic modulus of the particles of the order of $Y \sim k_n/R_0 = 20$ GPa, which is a reasonable value for rocks. The value of γ is chosen so that the linear coefficient of restitution is $e = 0.45$ (see Appendix 1), in the lower range of experimental measurements [*Chau et al.*, 2002].

The tensile strength within the cohesive column can be estimated by

$$\sigma_T = \frac{C}{\pi {R_0}^2} = \frac{m_0 g \mathrm{Bo}}{\pi {R_0}^2} \tag{7}$$

Table 4 gives the corresponding value of σ_T for increasing values of the Bond number. The case Bo = 0 corresponds to an infinitely fragile material (such as sand in experiments). The values of σ_T obtained for Bo varying from 10 to 100 correspond to the lower range of tensile strengths measured for samples of artificial rock, mudstone, and sandstone by *Sklar and Dietrich* [2001]. Even if these values are relatively low, they are only 1 order of magnitude smaller than the maximum stress below the column (see Table 2). Let us keep in mind that our estimate of σ_T does not represent the microscopic strength of a small rock sample but rather the average effective strength within the column (taking into account the possible existence of fractures before failure). It is therefore representative of both the intrinsic mechanical properties of the rock and the state of weakening within the cliff.

The limitation of the model is that the size of unit particles constitutes a cutoff length for fragmentation: once a cohesive block has been reduced to a single particle, it cannot be further fragmented. This intrinsically reduces the influence of the fragmentation process during the flow. However, reducing the size of the unit particles would require both increasing the total number of particles (in order to produce a column of realistic height) and reducing the iterative time step (for a given stiffness k_n, the collision duration τ_c roughly scales like $\sqrt{m_0}$, as shown in Appendix 1). The particle size that we adopted constitutes a fair compromise in order to limit the total computational time while preserving realistic values for Y and H_0.

Table 3. Mechanical Properties of the Unit Particles (See Sections 2.2.1 and 2.3)

Parameter	Value in the Simulation
Radius	$R_0 = 0.5$ m
Normal elastic constant	$k_n = 10^{10}$ N m^{-1}
Effective viscous constant	$\gamma = 1.810^6$ N m^{-1} s
Tangential elastic constant	$k_t = 2/7k_n$
Young's modulus	$Y = 20$ GPa
Friction coefficient	$\mu = 0.6$
Restitution coefficient	$e = 0.45$

Table 4. Effective Tensile Strength of the Material as a Function of the Bond Number, for Particles of Mean Size $R_0 = 50$ cm (See Equation (7))

Bo	σ_T
10	0.16 MPa
50	0.8 MPa
100	1.6 MPa

3. Runout of the Avalanche

3.1. Dynamics of the Front

We define the front of the avalanche by the farthest particle that remains connected (by a particle-particle contact) to the main granular mass. At each time step, we normalize the runout $(x - L_0)$ by its final value $(L_\infty - L_0)$ and plot it as a function of time. Time is expressed in units of the free-fall timescale $\tau_{ff} = \sqrt{H_0/(2g)}$. For high values of the initial aspect ratio (see Figure 3), we observe that tensile bonds do not modify significantly the dynamics of the front, though the final state is reached slightly faster for large values of Bo (i.e., strong bonds). For a smaller aspect ratio, the dynamics remain similar at low Bond numbers. However, when the tensile strength is higher (Bo > 20) the dynamics are qualitatively very different: the total duration of the collapse can be increased by up to a factor 200. After a static period of variable duration, the column fails and collapses rapidly: after only a few percent of the total collapse duration, the runout has reached about 60% of its final value. This rapid fall is followed by a slow adjustment of the deposit, large blocks being carried forward on top of a layer of fine fragments (see section 4.2).

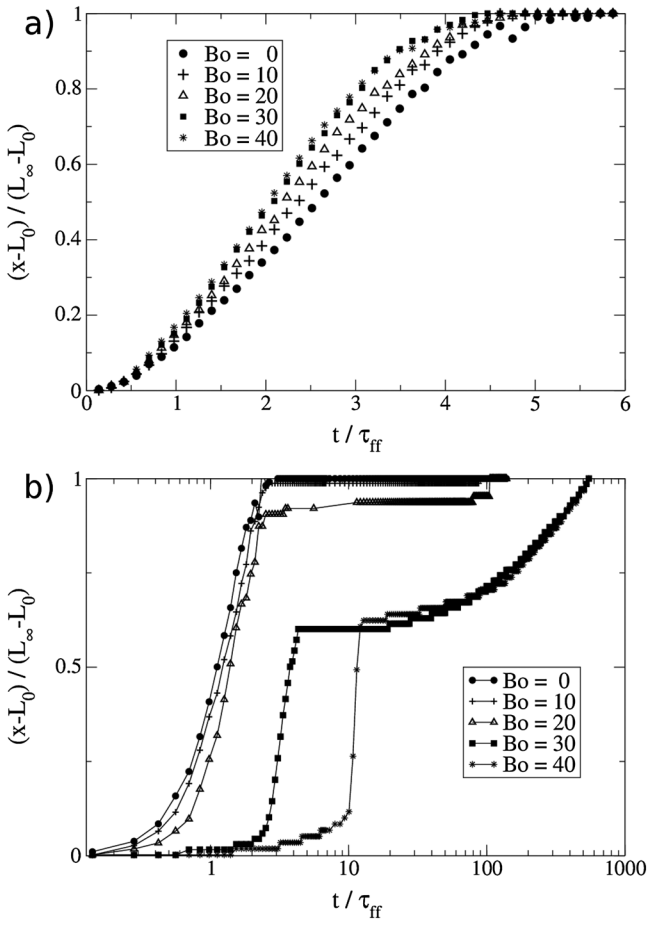

Figure 3. Normalized position of the front of the avalanche as a function of time (normalized by the free-fall timescale) for different values of the Bond number: (a) for an initial aspect ratio $a = 16.1$ and (b) for $a = 0.61$ (note the logarithmic scale for time).

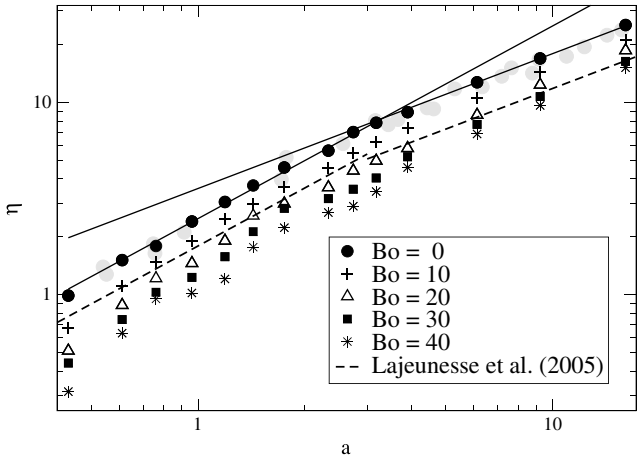

Figure 4. Normalized runout distance of the flow $\eta = (L_\infty - L_0)/L_0$ as a function of the initial aspect ratio of the column $a = H_0/L_0$. Straight lines represent power law fits for Bo = 0 (cf. equation (8)). Grey disks are data obtained numerically with the contact dynamics method (at Bo = 0) by *Staron and Hinch* [2005], shown for comparison. Dashed lines are data obtained in a quasi-2-D experiment [*Lajeunesse et al.*, 2005].

3.2. Scaling Laws for the Runout Distance

We normalize the runout distance by the initial width of the column $\eta = (L_\infty - L_0)/L_0$ and plot it as a function of the initial aspect ratio a (see Figure 4).

We find that for Bo = 0 (i.e., zero bond strength and effectively a granular material) the runout distance follows two different power laws, depending on the aspect ratio:

$$\eta_0 = \begin{cases} 2.5a & \text{for} \quad a \leq 3 \\ 3.6a^{0.7} & \text{for} \quad a \geq 3 \end{cases} \tag{8}$$

As illustrated in Figure 4, our results are in very good agreement with previous numerical findings by *Staron and Hinch* [2005]. The exponents of the power laws are also compatible with the results of pseudo-2-D experiments by *Lajeunesse et al.* [2005]. However, as was already noted by *Roche et al.* [2011], the runout that we obtain numerically is systematically about 1.5 times higher than in experiments. This is likely due to the fact that friction is higher in these experiments than in our simulations: on one hand, because the grains are confined between two frictional glass plates [*Taberlet et al.*, 2008] and on the other hand, because the third dimension induces transverse motion, which is responsible for an increase in effective friction, as shown numerically by *Hazzard and Mair* [2003].

Figure 4 shows that for a nonzero Bond number, the runout distance follows the same trend as for Bo = 0. However, we observe that an increase of the Bond number (that is, of the tensile strength) always leads to a decrease of the runout distance: for a given aspect ratio, a rockslide originating in a more fragile cliff will travel a longer distance. The granular case (Bo = 0), which corresponds to an infinitely fragile material ($\sigma_T = 0$), gives the upper limit η_0 of the runout distance.

3.3. Fragmentation Dynamics

The dynamics of rock fragmentation can be followed along the flow by computing at each time step the number and size of produced fragments (that is, blocks of particles that are still held together by the tensile bonds). We compute in particular the number of fine fragments, that is, those that are reduced to a unit spherical particle (and cannot be further split).

The evolution of the volumetric fraction ϵ constituted by these fine particles, normalized by its final value ϵ_∞, is plotted in Figure 5. When significantly larger than 1, the Bond number does not have much influence on the dynamics of fragmentation. Two phases can be observed before ϕ reaches its final value. Until time $t_1 \simeq 2\tau_{\text{ff}}$ (phase 1), ϵ increases rapidly: its evolution can be fitted by $\epsilon(t) \propto t^{2.7}$. At $t = t_1$, the runout is only 40% of its final value but 80% of the final number of fine fragments have already been produced (see Figure 3). Most of them are produced along the slip surface. In phase 2, they are produced at a much slower rate, with $\epsilon(t) \propto t^{0.2}$, and mostly in the basal layer of the flowing material. The final number of fine fragments is reached slightly before the end of the flow.

4. Properties of the Deposit

4.1. Internal Structure

We can characterize the deposit by the vertical origin of each particle. Figure 6 represents the aspect of the deposit for a moderate initial aspect ratio and three values of the Bond number. A color is attributed to each particle, based on its initial vertical position in the column. When the Bond number is increased, the surface of the deposit is less smooth and presents larger irregularities than in the granular case. In the granular case (Bo = 0), the deposit preserves the initial stratigraphic structure: material found at the surface comes almost

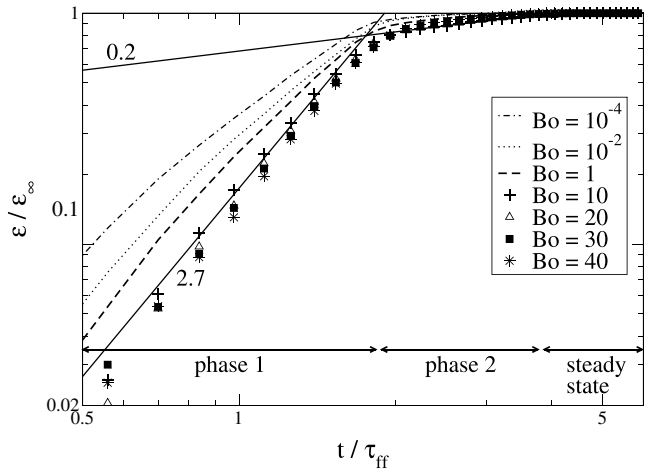

Figure 5. Volumetric fraction of fine fragments as a function of time for $a = 16.1$ and different values of the Bond number. Two power law fits for phases 1 and 2 are indicated with their respective indices.

entirely from the upper part of the column. As the material's strength is increased, tilted blocks appear and some material that originates from the inner layers of the column can outcrop at the surface of the deposit.

4.2. Grain Size Distribution

Let us now examine the sedimentary fabric within the deposit (see Figure 7): we attribute to each block a color that depends on its volume, expressed as the number of unit particles that it contains (the hue scale in the figure is logarithmic). Whatever the material's strength, the final deposit consists of rafted large blocks laying on a matrix of fine-grained material, as is observed in many natural deposits for rockslides or pyroclastic flows [*Cruden and Hungr*, 1986; *Hewitt*, 1988; *Yarnold*, 1993; *Davies et al.*, 1999; *Bernard et al.*, 2009]. Though large blocks can be found over the whole length of the deposit, the size of outcropping fragments can vary significantly in a single event, large blocks being separated by fine-grained material. For Bo = 10, the largest blocks have a characteristic size $R_{max} \sim 10$ m and for Bo = 30 up to $R_{max} \sim 20$ m. This is consistent with the very wide size distributions observed at the surface of natural events (ranging from sandy or silty fines to blocks larger than 100 m^3) [*Evans et al.*, 2006]. For Bo > 40, the material does not get much fragmented and the size of the largest block is comparable to the column's height.

Let us finally remark that the apparent size sorting from top to bottom of the deposit is not caused by the granular dynamics (as in the "Brazil nut effect" where vibrations allow small grains to migrate down a network of larger grains [*Möbius et al.*, 2001]) but results from the fact that superficial blocks are subject to less stress and can therefore remain roughly intact: by following their trajectories, we did not observe any significant vertical migration of the large blocks during the collapse.

We now compute the final grain size distribution within the deposit. To this effect we only take into account particles that have been displaced by more than 10 R_0. Hence, the static part of the column (which has not been affected by the collapse) does not appear in the distribution. Figure 8 represents the volumetric fraction of the deposit that is composed of fragments smaller than a given size, for the aspect ratio $a = 2.74$. It shows

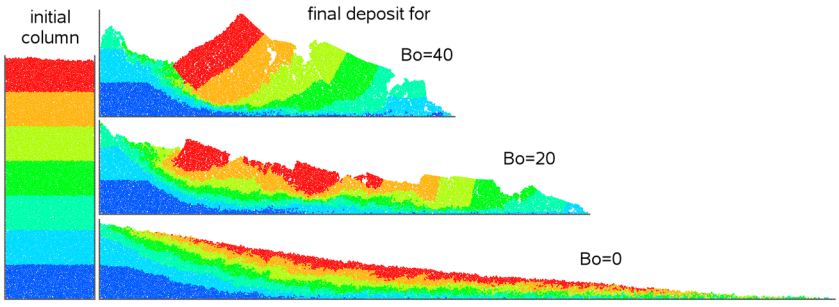

Figure 6. Granular column of aspect ratio $a = 2.74$, and its deposit after collapse, for three values of the Bond number. Color indicates the original vertical position of particles.

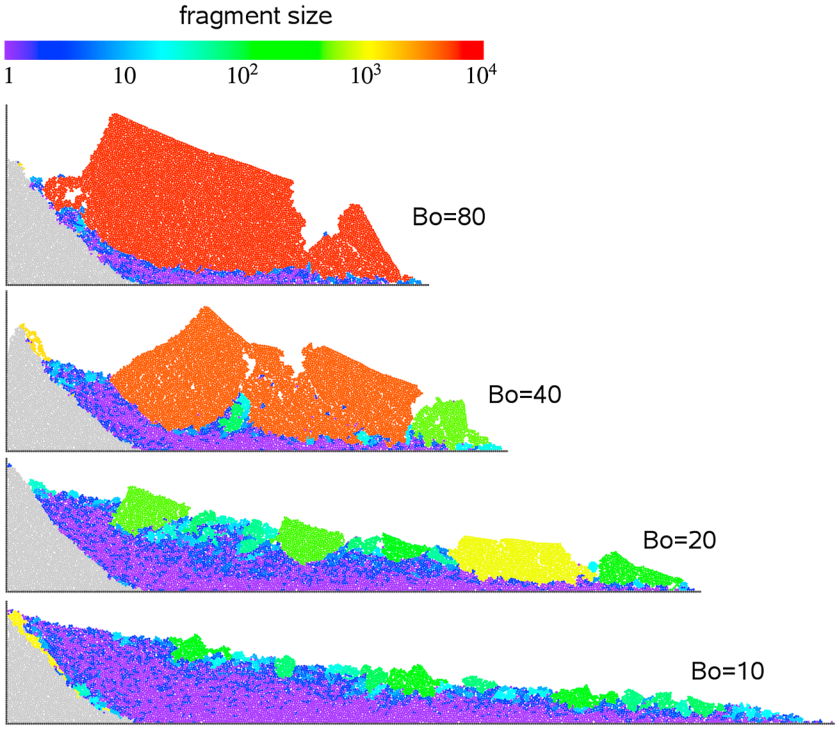

Figure 7. Aspect of the final deposit, for $a = 2.74$ and four values of the Bond number. The logarithmic hue scale indicates the size of each fragment, expressed as the number of unit particles it contains. Deposits consist of large blocks (green to red) laying over a layer of very fine particles (purple). The gray part is the fraction of the column that has not been affected by the collapse (whose particles have been displaced by less than 10 R_0).

that for an increasing strength of the material, the fraction of small fragments diminishes, whereas the size of the largest fragments found in the deposit increases. For a very brittle material (Bo $\sim$ 10–20), the distribution is relatively well graded. By contrast for Bo > 40 the distribution tends to be bimodal, with roughly 75% of the deposit made of fragments larger than 4000 particles and 25% or less of small (< 10 particles) fragments.

Following *Hardin* [1985] and *Bowman et al.* [2012], we define the degree of fragmentation within the deposit as

$$\Phi = \frac{A}{A_0} \tag{9}$$

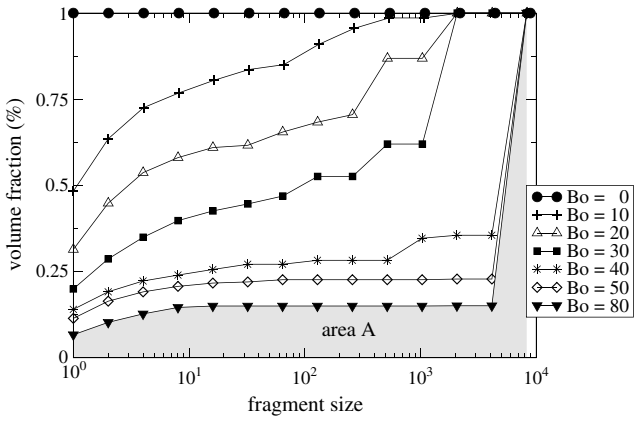

Figure 8. Cumulative grain size distribution in the deposit, for an aspect ratio $a = 2.74$ and different values of Bo. The size of a fragment is expressed as the number of unit particles that it contains. The area A of the gray surface corresponds to the integral of the distribution for Bo = 80.

where A is the area below the granulometric curve (colored in gray, for the case Bo = 80, in Figure 8) and A_0 is the potential breakage, that is, the area that would be obtained if the deposit was entirely composed of unit particles (which happens in the granular case Bo = 0). Contrary to the Bond number, the degree of fragmentation is a quantity that can be directly deduced from the observation of a deposit (whether in experiments [*Bowman et al.*, 2012] or in the field), provided that one chooses a minimal fragment size (for instance, *Hardin* [1985] defines it as a silt size of 0.074 mm though fragments as small as 10 nm can be found in deposits).

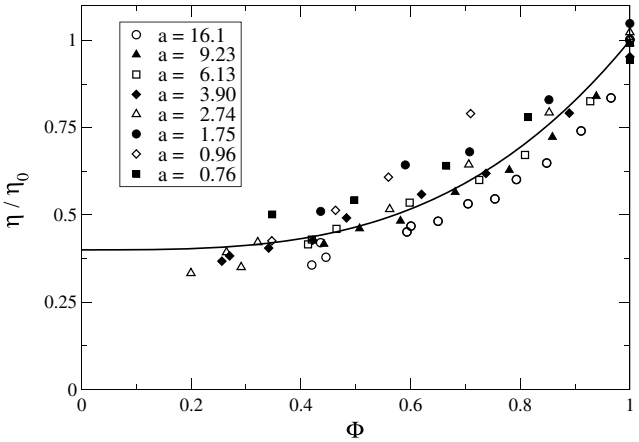

Figure 9. Runout distance η normalized by its value η_0 in the case of total fragmentation (Bo = 0 or $\Phi = 1$), as a function of the degree of fragmentation Φ and for different aspect ratios of the column. The black line is the empirical fit $\eta = \eta_0 \left(0.4 + 0.6\Phi^{3.2}\right)$.

In Figure 9, we plot again the runout distance, normalized by the value η_0 obtained for Bo = 0 and $\Phi = 1$ (cf. equation (8)), as a function of the degree of fragmentation. A unique global tendency can be observed despite the small dependence on the aspect ratio a. For any aspect ratio, the runout distance increases monotonically with the degree of fragmentation, the granular case being the upper limit. The causality of this relation is, however, difficult to assess: one can argue either that fragmentation increases runout or that a longer runout gives more opportunity for fragmentation. Let us insist, furthermore, that the parameter Φ only reflects the state of fragmentation within the deposit and not the dynamical process. We propose the following empirical fit for the runout distance, for which we do not have any satisfactory explanation:

$$\eta = \left(0.4 + 0.6\Phi^{3.2}\right) \times \begin{cases} 2.5a & \text{for} \quad a \leq 3 \\ 3.6a^{0.7} & \text{for} \quad a \geq 3 \end{cases} \tag{10}$$

One must note that the state of zero fragmentation is hardly reachable in simulations if the column actually collapses, which makes the prediction essentially valid in the region $0.2 \leq \Phi \leq 1$. This range is reasonable when compared to values measured in the field: for instance, *Bowman et al.* [2012] review values of the relative breakage ranging from 0.34 to 0.58 for four cases of various volumes. The case $\Phi = 1$ is ambiguous: indeed, this corresponds to the limit of total fragmentation (the deposit consists only of single particles). However, this limit is obtained for Bo = 0, that is, when the column is already entirely fragmented before collapsing: in practice, no bonds are created nor broken between particles. In order to resolve this apparent contradiction, we verified that the collapse of a column made of a very weak material (that is, for $\mathrm{Bo} = 10^{-4} \rightarrow 1$) leads to the same deposit as the granular column and to an entirely fragmented deposit. The case of total fragmentation is therefore indeed obtained in the regime Bo$\rightarrow$ 0 and constitutes the upper limit of the runout distance.

5. Discussion and Conclusions

We have presented the results of a numerical study of the collapse of a brittle granular column. These simulations mimic classical granular collapse experiments but include the effect of a nonzero material's tensile strength and subsequent dynamic fragmentation. The discrete element method allows us to model within the same simulation the different phases (failure, collapse, and horizontal spreading) and to account explicitly for the breakage of the material into smaller and smaller fragments. We have verified that the runout obtained with no tensile bonds is identical to the values obtained in existing studies using a different numerical method [*Staron and Hinch*, 2005] and comparable to experimental values [*Lajeunesse et al.*, 2005]. When the strength of the material is increased, the normalized runout distance decreases but still follows the same trend as a function of the initial aspect ratio of the column. We show that the deposits become qualitatively very different when the material's strength is increased. A granular deposit is very smooth and preserves the stratigraphic structure of the initial column. By contrast, when the material is stronger, the deposit is rough and consists of a few large blocks laying on top of a thick layer made of very small fragments, as has been observed in natural events [*Cruden and Hungr*, 1986; *Hewitt*, 1988; *Yarnold*, 1993; *Davies et al.*, 1999; *Bernard et al.*, 2009]. The higher the material's strength, the more bimodal the grain size distribution becomes. The internal structure of the deposit is much disturbed: some material from the inner layers of the column can be found at the surface. Even if large blocks can be found everywhere at the surface of the deposit, their distribution remains very heterogeneous (in some points, the matrix of fine-grained material is observed to outcrop).

Finally, we computed the degree of fragmentation in the deposit, following the definition by *Hardin* [1985]. This quantity increases with the aspect ratio of the column but reduces when the material's tensile strength is increased. As a consequence, for a given aspect ratio the runout distance of the avalanche increases with the degree of fragmentation in the deposit, as proposed by *Davies et al.* [1999, 2010] and observed by *Bowman et al.* [2012]. One must note, though, that the granular case (which corresponds to total fragmentation $\Phi = 1$) constitutes the upper limit for the runout, which means that dynamic fragmentation cannot explain that large rock avalanches travel about twice longer than predicted in experiments with (nonfragmenting) sand grains or glass beads. This implies that either our model for fragmentation is yet too simplistic or the fragmentation process is not responsible for the long runout and an additional mechanism should be invoked (e.g., mass entrainment during the flow). However, it also implies that if a slope fails, the runout will be larger if the material is already highly weakened before its failure. For a given aspect ratio of the column, we predict that the runout distance is about twice longer in the case of total fragmentation ($\Phi = 1$) than if the degree of fragmentation in the deposit reaches only $\Phi = 0.5$.

We have shown that our simulations compare well with experiments and existing numerical studies dealing with granular materials and are effective in capturing the effects of dynamic fragmentation during the flow. However, in order to compare more directly the results with the characteristics of natural events, the same numerical model is easily extendable to a different geometry, that is, the three-dimensional flow of a mass along an incline [*Manzella and Labiouse*, 2009; *Mollon et al.*, 2012], which allows to study the lateral spreading of an avalanche. The extension of our model to three dimensions requires, however, to adopt a more accurate description of bonds (for instance, by considering Euler-Bernoulli beams, as in *Carmona et al.* [2008]), allowing them to fail not only in elongation but also in bending and torsion, which introduces many more control parameters to the model. Taking these modes of failure into account might reduce locally the friction between bonded sliding particles and avoid obtaining unrealistically shaped blocks, but it should not modify the qualitative influence of material strength that we have evidenced in this study. The influence of such a fragmentation on effective friction will be the object of a further publication. Having added tensile bonds in the material would also allow us to start from a stable slope and study the effect of a sudden destabilizing perturbation (for example, a local loss of rigidity in the column), which is more realistic than the spontaneous collapse of a vertical column.

Appendix A: Numerical Methods

The Verlet algorithm is used to implement time integration of Newton's equations of motion: knowing the position of a particle at times t and $t - \Delta t$ and its acceleration $\mathbf{a}$ at time t allows us to compute its position at time $t + \Delta t$:

$$\mathbf{r}(t + \Delta t) = 2\mathbf{r}(t) - \mathbf{r}(t - \Delta t) + \Delta t^2 \mathbf{a}(t) \tag{A1}$$

By using this approximation, the numerical error at each time step is of the order of Δt^4. The acceleration of the particle can be computed from the sum of all forces that it experiences:

$$\mathbf{a}(t) = \mathbf{g} + \frac{1}{m} \sum_{\text{contacts}} \mathbf{F}(t) \tag{A2}$$

The same method is applied to integrate the equation for rotational motion: $\theta(t)$ being the angular position of the particle,

$$\theta(t + \Delta t) = 2\theta(t) - \theta(t - \Delta t) + \frac{\Delta t^2}{I} \sum_{\text{contacts}} \mathcal{M}(t) \tag{A3}$$

with $I = \frac{2}{5} m R^2$ the moment of inertia of the particle and $\mathcal{M}$ the torque of each contact force acting on the particle.

In order to compute adequately each collision between particles, the iterative time step is chosen as $\Delta t = \tau_c / 100$, with τ_c the typical duration of a collision between particles:

$$\tau_c = \pi \frac{\sqrt{m_0 / k_n}}{\sqrt{1 - \beta^2}} \quad \text{with} \quad \beta^2 = \frac{\gamma^2}{4\, m_0\, k_n} \tag{A4}$$

In a collision between particles *i* and *j* with respective angular velocities $\boldsymbol{\Omega}_i$ and $\boldsymbol{\Omega}_j$, the sliding velocity at the contact point is defined as

$$\mathbf{v}_{ij}^{\,s} = \mathbf{v}_{ij} - \left(\mathbf{v}_{ij} \cdot \mathbf{n}_{ij}\right) \mathbf{n}_{ij} + R_j \boldsymbol{\Omega}_j - R_i \boldsymbol{\Omega}_i \tag{A5}$$

with $\mathbf{v}_{ij} = \mathbf{v}_j - \mathbf{v}_i$ the relative velocity between particles.

The coefficient of restitution for a collision between two particles of identical radii can be expressed as [*Schäfer et al.*, 1996]

$$e = \exp\left[-\pi \frac{\beta}{\sqrt{1-\beta^2}}\right] \tag{A6}$$

Acknowledgments
Data supporting the results of this article can be obtained by contacting Vincent Langlois (vincent.langlois@univ-lyon1.fr). V.L. would like to thank the members of the CNRS GdR TransNat for their fruitful discussions and Y. Ricard for his suggestions about this work. The authors would like to acknowledge the insightful input of anonymous referees as well as the Associate Editor on this article.

References

Abe, S., and K. Mair (2005), Grain fracture in 3D numerical simulations of granular shear, *Geophys. Res. Lett.*, *32*, L05305, doi:10.1029/2004GL022123.

Allemand, P., C. Delacourt, E. Lajeunesse, O. Devauchelle, and F. Beauducel (2014), Erosive effects of the storm Helena (1963) on Basse Terre Island (Guadeloupe-Lesser Antilles Arc), *Geomorphology*, *206*, 79–86.

Artoni, R., A. C. Santomaso, F. Gabrieli, D. Tono, and S. Cola (2013), Collapse of quasi-two-dimensional wet granular columns, *Phys. Rev. E*, *87*(3), 032205, doi:10.1103/PhysRevE.87.032205.

Balmforth, N. J., and R. R. Kerswell (2005), Granular collapse in two dimensions, *J. Fluid Mech.*, *538*, 399–428, doi:10.1017/S0022112005005537.

Bernard, B., B. Wyk de Vries, and H. Leyrit (2009), Distinguishing volcanic debris avalanche deposits from their reworked products: The Perrier sequence (French Massif Central), *Bull. Volcanol.*, *71*(9), 1041–1056, doi:10.1007/s00445-009-0285-7.

Bi, W., R. Delannay, P. Richard, N. Taberlet, and A. Valance (2005), Two- and three-dimensional confined granular chute flows: Experimental and numerical results, *J. Phys. Condens. Matter*, *17*(24), S2457.

Bowman, E., W. Take, K. Rait, and C. Hann (2012), Physical models of rock avalanche spreading behaviour with dynamic fragmentation, *Can. Geotech. J.*, *476*, 460–476, doi:10.1139/T2012-007.

Carmona, H., F. Wittel, F. Kun, and H. Herrmann (2008), Fragmentation processes in impact of spheres, *Phys. Rev. E*, *77*(5), 051302.

Chau, K., R. Wong, and J. Wu (2002), Coefficient of restitution and rotational motions of rockfall impacts, *Int. J. Rock Mech. Min. Sci.*, *39*(1), 69–77.

Collins, G. S., and H. J. Melosh (2003), Acoustic fluidization and the extraordinary mobility of sturzstroms, *J. Geophys. Res.*, *108*(B10), 2473, doi:10.1029/2003JB002465.

Crosta, G. B., P. Frattini, and N. Fusi (2007), Fragmentation in the Val Pola rock avalanche, Italian Alps, *J. Geophys. Res.*, *112*, F01006, doi:10.1029/2005JF000455.

Crosta, G. B., S. Imposimato, and D. Roddeman (2009), Numerical modeling of 2-D granular step collapse on erodible and nonerodible surface, *J. Geophys. Res.*, *114*, F03020, doi:10.1029/2008JF001186.

Cruden, D. M., and O. Hungr (1986), The debris of the Frank Slide and theories of rockslide-avalanche mobility, *Can. J. Earth Sci.*, *23*(3), 425–432, doi:10.1139/e86-044.

Cundall, P. A., and O. D. L. Strack (1979), A discrete numerical model for granular assemblies, *Géotechnique*, *29*(1), 47–65.

Davies, T., and M. McSaveney (2009), The role of rock fragmentation in the motion of large landslides, *Eng. Geol.*, *109*(1-2), 67–79, doi:10.1016/j.enggeo.2008.11.004.

Davies, T., M. McSaveney, and R. Beetham (2006), Rapid block glides: Slide-surface fragmentation in New Zealand's Waikaremoana landslide, *Q. J. Eng. Geol. Hydrogeol.*, *39*(2), 115–129.

Davies, T., M. McSaveney, and K. Kelfoun (2010), Runout of the Socompa volcanic debris avalanche, Chile: A mechanical explanation for low basal shear resistance, *Bull. Volcanol.*, *72*, 933–944, doi:10.1007/s00445-010-0372-9.

Davies, T. R. (1982), Spreading of rock avalanche debris by mechanical fluidization, *Rock Mech.*, *15*(1), 9–24.

Davies, T. R., M. J. McSaveney, and K. Hodgson (1999), A fragmentation-spreading model for long-runout rock avalanches, *Can. Geotech. J.*, *36*(6), 1096–1110, doi:10.1139/t99-067.

De Blasio, F. V., and A. Elverhøi (2008), A model for frictional melt production beneath large rock avalanches, *J. Geophys. Res.*, *113*, F02014, doi:10.1029/2007JF000867.

Doyle, E. E., H. E. Huppert, G. Lube, H. M. Mader, and R. S. J. Sparks (2007), Static and flowing regions in granular collapses down channels: Insights from a sedimenting shallow water model, *Phys. Fluids*, *19*(10), 106601, doi:10.1063/1.2773738.

Evans, S., G. S. Mugnozza, A. Strom, R. Hermanns, A. Ischuk, and S. Vinnichenko (2006), Landslides from massive rock slope failure and associated phenomena, in *Landslides From Massive Rock Slope Failure*, pp. 03–52, Springer, Netherlands.

Fauque, L., and M. Strecker (1988), Large rock avalanches (Sturzströme, sturzstorms) at Sierra Aconquija, northern Sierras Pampeanas, Argentina, *Eclogae Geol. Helv.*, *81*, 579–592.

Gercek, H. (2007), Poisson's ratio values for rocks, *Int. J. Rock Mech. Min. Sci.*, *44*(1), 1–13.

Glicken, H. (1998), Rockslide-debris avalanche of May 18, 1980, Mount St. Helens Volcano, Washington, *Bull. Geol. Surv. Jpn.*, *49*, 55–106.

Gross, S. P., J. Fineberg, M. Marder, W. McCormick, and H. L. Swinney (1993), Acoustic emissions from rapidly moving cracks, *Phys. Rev. Lett.*, *71*(19), 3162–3165.

Hardin, B. O. (1985), Crushing of soil particles, *J. Geotech. Eng.*, *111*(10), 1177–1192.

Hazzard, J. F., and K. Mair (2003), The importance of the third dimension in granular shear, *Geophys. Res. Lett.*, *30*(13), 1708, doi:10.1029/2003GL017534.

Hewitt, K. (1988), Catastrophic landslide deposits in the Karakoram Himalaya, *Science*, *242*(4875), 64–67.

Hewitt, K., J. J. Clague, and J. F. Orwin (2008), Legacies of catastrophic rock slope failures in mountain landscapes, *Earth Sci. Rev.*, *87*(1), 1–38.

Jop, P., Y. Forterre, and O. Pouliquen (2006), A constitutive law for dense granular flows, *Nature*, *441*, 727–730.

Kelfoun, K., and T. H. Druitt (2005), Numerical modeling of the emplacement of Socompa rock avalanche, Chile, *J. Geophys. Res.*, *110*, B12202, doi:10.1029/2005JB003758.

Kelfoun, K., P. Samaniego, P. Palacios, and D. Barba (2009), Testing the suitability of frictional behaviour for pyroclastic flow simulation by comparison with a well-constrained eruption at Tungurahua volcano (Ecuador), *Bull. Volcanol.*, *71*, 1057–1075, doi:10.1007/s00445-009-0286-6.

Lacaze, L., J. C. Phillips, and R. R. Kerswell (2008), Planar collapse of a granular column: Experiments and discrete element simulations, *Phys. Fluids*, *20*(6), 063302.
Lagrée, P.-Y., L. Staron, and S. Popinet (2011), The granular column collapse as a continuum: Validity of a two-dimensional Navier-Stokes model with a μ(I)-rheology, *J. Fluid Mech.*, *686*, 378–408, doi:10.1017/jfm.2011.335.
Lajeunesse, E., A. Mangeney-Castelnau, and J. P. Vilotte (2004), Spreading of a granular mass on a horizontal plane, *Phys. Fluids*, *16*(7), 2371–2381, doi:10.1063/1.1736611.
Lajeunesse, E., J. B. Monnier, and G. M. Homsy (2005), Granular slumping on a horizontal surface, *Phys. Fluids*, *17*(10), 103302, doi:10.1063/1.2087687.
Lajeunesse, E., C. Quantin, P. Allemand, and C. Delacourt (2006), New insights on the runout of large landslides in the Valles-Marineris canyons, Mars, *Geophys. Res. Lett.*, *33*, L04403, doi:10.1029/2005GL025168.
Larrieu, E., L. Staron, and E. J. Hinch (2006), Raining into shallow water as a description of the collapse of a column of grains, *J. Fluid Mech.*, *554*, 259–270, doi:10.1017/S0022112005007974.
Legros, F. (2002), The mobility of long-runout landslides, *Eng. Geol.*, *63*, 301–331, doi:10.1016/S0013-7952(01)00090-4.
Lin, G.-W., H. Chen, N. Hovius, M.-J. Horng, S. Dadson, P. Meunier, and M. Lines (2008), Effects of earthquake and cyclone sequencing on landsliding and fluvial sediment transfer in a mountain catchment, *Earth Surf. Processes Landforms*, *33*(9), 1354–1373.
Locat, P., R. Couture, S. Leroueil, J. Locat, and M. Jaboyedoff (2006), Fragmentation energy in rock avalanches, *Can. Geotech. J.*, *43*(8), 830–851.
Lube, G., H. E. Huppert, R. S. J. Sparks, and M. A. Hallworth (2004), Axisymmetric collapses of granular columns, *J. Fluid Mech.*, *508*, 175–199, doi:10.1017/S0022112004009036.
Lumay, G., and N. Vandewalle (2010), Flow of magnetized grains in a rotating drum, *Phys. Rev. E*, *82*, 040301, doi:10.1103/PhysRevE.82.040301.
Mangeney, A., L. S. Tsimring, D. Volfson, I. S. Aranson, and F. Bouchut (2007), Avalanche mobility induced by the presence of an erodible bed and associated entrainment, *Geophys. Res. Lett.*, *34*, L22401, doi:10.1029/2007GL031348.
Mangeney-Castelnau, A., J.-P. Vilotte, M. Bristeau, B. Perthame, F. Bouchut, C. Simeoni, and S. Yerneni (2003), Numerical modeling of avalanches based on Saint-Venant equations using a kinetic scheme, *J. Geophys. Res.*, *108*(2527), doi:10.1029/2002JB002024.
Manzella, I., and V. Labiouse (2009), Flow experiments with gravel and blocks at small scale to investigate parameters and mechanisms involved in rock avalanches, *Eng. Geol.*, *109*(1), 146–158.
Mason, T. G., A. J. Levine, D. Ertaş, and T. C. Halsey (1999), Critical angle of wet sandpiles, *Phys. Rev. E*, *60*, R5044–R5047, doi:10.1103/PhysRevE.60.R5044.
McCarthy, J. J., D. V. Khakhar, and J. M. Ottino (2000), Computational studies of granular mixing, *Powder Technol.*, *109*(1), 72–82.
McSaveney, M., and T. Davies (2009), Surface energy is not one of the energy losses in rock comminution, *Eng. Geol.*, *109*, 109–113, doi:10.1016/j.enggeo.2008.11.001.
Mériaux, C., and T. Triantafillou (2008), Scaling the final deposits of dry cohesive granular columns after collapse and quasi-static fall, *Phys. Fluids*, *20*, 033301.
Métayer, J.-F., P. Richard, A. Faisant, and R. Delannay (2010), Electrically induced tunable cohesion in granular systems, *J. Stat. Mech: Theory Exp.*, *2010*(08), P08003.
Möbius, M. E., B. E. Lauderdale, S. R. Nagel, and H. M. Jaeger (2001), Brazil-nut effect: Size separation of granular particles, *Nature*, *414*, 270.
Mollon, G., V. Richefeu, P. Villard, and D. Daudon (2012), Numerical simulation of rock avalanches: Influence of a local dissipative contact model on the collective behavior of granular flows, *J. Geophys. Res.*, *117*, F02036, doi:10.1029/2011JF002202.
Moreau, J.-J. (1994), Some numerical methods in multibody dynamics: Application to granular materials, *Eur. J. Mech. A. Solids*, *13*, 93–114.
Morgan, J., and P. McGovern (2005a), Discrete element simulations of gravitational volcanic deformation: 1. Deformation structures and geometries, *J. Geophys. Res.*, *110*, B05402, doi:10.1029/2004JB003252.
Morgan, J., and P. McGovern (2005b), Discrete element simulations of gravitational volcanic deformation: 2. Mechanical analysis, *J. Geophys. Res.*, *110*, B05403, doi:10.1029/2004JB003253.
Nase, S. T., W. L. Vargas, A. A. Abatan, and J. McCarthy (2001), Discrete characterization tools for cohesive granular material, *Powder Technol.*, *116*(2), 214–223.
Pöschel, T., and T. Schwager (2005), *Computational Granular Dynamics: Models and Algorithms*, Springer-Verlag, Berlin.
Restagno, F., L. Bocquet, and E. Charlaix (2004), Where does a cohesive granular heap break?, *Eur. Phys. J. E*, *14*(2), 177–83, doi:10.1140/epje/i2004-10013-5.
Reznichenko, N. V., T. R. Davies, J. Shulmeister, and S. H. Larsen (2012), A new technique for identifying rock avalanche—Sourced sediment in moraines and some paleoclimatic implications, *Geology*, *40*(4), 319–322.
Robinson, T. R., T. R. Davies, N. V. Reznichenko, and G. P. De Pascale (2014), The extremely long-runout Komansu rock avalanche in the Trans Alai range, Pamir Mountains, southern Kyrgyzstan, *Landslides*, *12*, 523–535.
Roche, O., M. Gilbertson, J. Phillips, and R. Sparks (2005), Inviscid behaviour of fines-rich pyroclastic flows inferred from experiments on gas-particle mixtures, *Earth Planet. Sci. Lett.*, *240*(2), 401–414, doi:10.1016/j.epsl.2005.09.053.
Roche, O., M. Attali, A. Mangeney, and A. Lucas (2011), On the run-out distance of geophysical gravitational flows: Insight from fluidized granular collapse experiments, *Earth Planet. Sci. Lett.*, *311*(3-4), 375–385, doi:10.1016/j.epsl.2011.09.023.
Rognon, P., J.-N. Roux, M. Naaïm, and F. Chevoir (2008), Dense flows of cohesive granular materials, *J. Fluid Mech.*, *596*, 21–47.
Savage, S., and K. Hutter (1991), The dynamics of avalanches of granular materials from initiation to runout. Part I: Analysis, *Acta Mechanica*, *86*, 201–223.
Schäfer, J., S. Dippel, and D. Wolf (1996), Force schemes in simulations of granular materials, *J. Phys. I France*, *6*, 5–20.
Schneider, J.-L., and R. V. Fisher (1998), Transport and emplacement mechanisms of large volcanic debris avalanches: Evidence from the northwest sector of Cantal Volcano (France), *J. Volcanol. Geotherm. Res.*, *83*(1), 141–165.
Sharon, E., S. P. Gross, and J. Fineberg (1996), Energy dissipation in dynamic fracture, *Phys. Rev. Lett.*, *76*(12), 2117.
Silbert, L., D. Ertas, G. Grest, and T. Halsey (2001), Granular flow down an inclined plane: Bagnold scaling and rheology, *Phys. Rev. E*, *64*, 051302.
Sklar, L. S., and W. E. Dietrich (2001), Sediment and rock strength controls on river incision into bedrock, *Geology*, *29*(12), 1087–1090.
Staron, L. (2008), Mobility of long-runout rock flows: A discrete numerical investigation, *Geophys. J. Int.*, *172*(1), 455–463, doi:10.1111/j.1365-246X.2007.03631.x.
Staron, L., and E. J. Hinch (2005), Study of the collapse of granular columns using two-dimensional discrete-grain simulation, *J. Fluid Mech.*, *545*, 1–27, doi:10.1017/S0022112005006415.
Taberlet, N., P. Richard, and R. Delannay (2008), The effect of sidewall friction on dense granular flows, *Comput. Math. Appl.*, *55*(2), 230–234.

Taylor, K., P. J. King, and M. R. Swift (2008), Influence of magnetic cohesion on the stability of granular slopes, *Phys. Rev. E*, *78*, 031304, doi:10.1103/PhysRevE.78.031304.

Thompson, E. L., and H. E. Huppert (2007), Granular column collapses: Further experimental results, *J. Fluid Mech.*, *575*, 177–186, doi:10.1017/S0022112006004563.

Ui, T., S. Kawachi, and V. E. Neall (1986), Fragmentation of debris avalanche material during flowage? Evidence from the Pungarehu Formation, Mount Egmont, New Zealand, *J. Volcanol. Geotherm. Res.*, *27*(3), 255–264.

Yarnold, J. C. (1993), Rock-avalanche characteristics in dry climates and the effect of flow into lakes: Insights from mid-Tertiary sedimentary breccias near Artillery Peak, Arizona, *Geol. Soc. Am. Bull.*, *105*(3), 345–360.

Zenit, R. (2005), Computer simulations of the collapse of a granular column, *Phys. Fluids*, *17*(3), 031703, doi:10.1063/1.1862240.